

NANO EXPRESS

Open Access



Highly Efficient Inverted Perovskite Solar Cells with CdSe QDs/LiF Electron Transporting Layer

Furui Tan^{1,2*}, Weizhe Xu^{1,2}, Xiaodong Hu^{1,2}, Ping Yu^{1,2} and Weifeng Zhang^{1,2}

Abstract

Organic/inorganic hybrid perovskite solar cell has emerged as a very promising candidate for the next generation of near-commercial photovoltaic devices. Here in this work, we focus on the inverted perovskite solar cells and have found that remarkable photovoltaic performance could be obtained when using cadmium selenide (CdSe) quantum dots (QDs) as electron transporting layer (ETL) and lithium fluoride (LiF) as the buffer, with respect to the traditionally applied and high-cost [6,6]-phenyl-C61-butyric acid methyl ester (PCBM). The easily processed and low-cost CdSe QDs/LiF double layer could facilitate convenient electron-transfer and collection at the perovskite/cathode interface, promoting an optoelectric conversion efficiency of as high as 15.1%, very close to that with the traditional PCBM ETL. Our work provides another promising choice on the ETL materials for the highly efficient and low-cost perovskite solar cells.

Keywords: Perovskite, Electron transport, Solar cell, Inverted structure, Quantum dot

Background

Hybrid organic-inorganic perovskite solar cell has been recognized as a very promising new-generation thin film solar cells based on remarkable improvement in its photovoltaic performance with a present efficiency of as high as 22.1% [1]. Long-term environmental stability could also be obtained with a time scale of several hundred to a thousand hours [2, 3]. In the large family of perovskite solar cells, planar heterojunction with an inverted device skeleton has been highly emphasized and intensively researched because of its appealing potential in mild fabrication process and easily accessible flexibility [4–7]. Typically for this device structure, the perovskite layer is sandwiched between the anode and cathode buffer layers to form a p-i-n-layered energy level alignment. In this structure, the n type layer plays a critical role in accepting electrons and inhibiting holes from the perovskite layer.

Up to now, a variety of semiconducting materials were adopted as electron transporting layer (ETL); the

traditional choice is the extensively used C₆₀ and its derivative, [6,6]-phenyl-C61-butyric acid methyl ester (PCBM) [7–10]. Through uniform and excellent electrical contact with the underlied perovskite film, the small molecule ETLs can provide remarkable efficiency of as high as 19.9% [10]. Although high efficiency was obtained for organic ETLs, gradual attention arises to the high cost of such ETL materials, the complicated device fabrication process, and the unsatisfied device stability. In comparison, ETL materials based on inorganic nanoparticles appeal great attention because of their potential advantage in low material cost, charge mobility, mild fabrication integration, and promising device stability [11–15]. However, up to now, exploring on inorganic ETLs in inverted structure was relatively rare. M. Grätzel and L. Han et al. developed highly conductive Nb-doped TiO₂ film on PCBM to obtain an efficiency of 16.2% with >90% retained PCE after 1000 h of light soaking [12]. Similarly, Alex K et al. introduced Zn₂SnO₄ nanocrystalline thin film on PCBM buffer layer to facilitate electron extraction and thus increased the device performance to 17.76% [14]. You et al. and Yang et al. firstly fabricated all-metal-oxide layer-based inverted perovskite solar cell that show 16.1% efficiency and significantly improved stability [15]. Generally,

* Correspondence: frtan@henu.edu.cn

¹Key Laboratory of Photovoltaic Materials, Henan University, Kaifeng 475004, China

²Department of Physics and Electronics, Henan University, Kaifeng 475004, China

either the quantity of reported works or the photovoltaic performance of this inverted devices lagged behind the traditional structure. More investigation on the inorganic ETL-based inverted perovskite solar cells are needed to accelerate the fast growth of this field.

Here in this work, we developed a novel all-inorganic ETL for the inverted perovskite solar cells, a cadmium selenide (CdSe) quantum dots (QDs)/lithium fluoride (LiF) double layer obtained from spin-coating and thereafter evaporation process. Up to now, the synthesis and optoelectric application of CdSe QDs have been extensively reported as electron acceptor [16–18]. Ultrathin and island-shaped LiF were also widely used in the cathode buffer layers in organic solar cells [19, 20]. All these well-developed references prompt us to consider them as inorganic ETL and cathode buffer layer in the inverted perovskite solar cells. We have found that the CdSe/LiF layer plays an excellent role in extracting and transferring electrons from the underlying perovskite to the above cathode, enabling a photovoltaic conversion efficiency of as high as 15.1% that is very close to the PCBM reference. Our work provides another promising choice on the low cost and all-inorganic electron extraction layer for inverted perovskite solar cells.

Methods

Synthesis of CdSe QDs

Cadmium oxide (CdO, 1 mmol), oleic acid (OA, 10 mmol), and 3 g trioctylphosphine oxide (TOPO) were dissolved in a four-neck round bottom flask and pumped at 140 °C under N₂ flow for 30 min. After that, the temperature was raised to about 280 °C during which the solution turned clear. A TOP-Se solution (containing 1 mmol Se in 3 ml tri-*n*-octylphosphine (TOP) was injected into the flask quickly. The reaction was allowed at 260 °C for 4 min, and then, the heating mantle was removed. After the solution was cooled to room temperature, 10 ml acetone was injected to collect the red precipitation by centrifugation at 4500 rpm. The obtained CdSe QDs were cleaned with chlorobenzene (CB)/acetone solvent/antisolvent for at least four times and then dissolved in 30 ml pyridine and stirred at 50 °C overnight to exchange the surface OA ligands. Then, the pyridine-capped CdSe QDs were collected by adding *n*-hexane to the solution and thereafter centrifuging at 4000 rpm. About 8 ml CB was used to disperse the collected CdSe QDs. The concentration of the final solution was adjusted to 15 mg/ml that was used for solar cell fabrication.

Device Fabrication

The pre-patterned indium tin oxide (ITO) glass was firstly ultrasonicated with deionized water, acetone, and isopropanol separately for 30 min and then dried by N₂

blowing. One hundred microliter poly(3,4-ethylenedioxythiophene) poly(styrene-sulfonate) (PEDOT:PSS, VPAI 4083) was spin-coated onto the ITO at 6000 rpm and then dried at 120 °C in air. The organic-inorganic perovskite solution was prepared by mixing 2 mmol MAI and 2 mmol PbI₂ in 1.6 ml DMF. The solution was stirred at 70 °C overnight in N₂-filled glovebox. The perovskite film was deposited on the substrate through a two-step spin-coating procedure (1000 rpm for 10 s and 6000 rpm for 30 s). One hundred eighty microliter chlorobenzene was deposited quickly at 5 s since the beginning of the second stage of spin-coating. All the perovskite films were annealed at 100 °C for 10 min. After cooling down, the as-prepared CdSe QD chlorobenzene solution was dripped on the perovskite surface, stayed for 5 s, and then spin-coated at different speed to obtain different film thickness. The substrate was transferred into thermal evaporator where a 0.8–1.0-nm LiF ultrathin film or particle islands was deposited (0.2 Å/s, 6 × 10⁻⁴ Pa) followed by 20 nm Au and 80 nm Ag. A mask was used to define six separate pixels each with an effective area of 0.04 cm².

Measurements

The film topology with and without CdSe/LiF covering were researched by field emission scanning electron microscope (FESEM, JEOL 7006F) and scanning probe microscope (SPA400). X-ray diffraction (XRD) was performed on a Rigaku D/max-gA X-ray diffractometer with Cu K α radiation. Light absorption properties were measured with ultraviolet-visible-inferred spectrophotometer (Varian Cary-5000). Photoluminescence (PL) spectra were collected on HORIBA Jobin Yvon Fluorlog-3 system. Time-resolved photoluminescence (TRPL) spectroscopy measurements were conducted using a pulse laser (512 nm) for excitation (F980 lifetime spectrometers, Edinburgh Instruments, EI). The TRPL decays at 790 nm were recorded by a time-correlated single-photon counting (TCSPC) spectrometer. The photovoltaic *I-V* properties were recorded on Keithley 2440 source meter combined with Newport 94043A solar simulator (AM 1.5 illumination). The unencapsulated solar cells were tested at room temperature in air. Typically, light soaking was needed to get a stabilize power conversion efficiency. External quantum efficiency (EQE) was measured on a solar cell IPCE measurement system (Crowntech QTest Station 500ADX) with a CM110 monochromator, a Keithley 2000 source meter, and a CT-TH-150 Br-W lamp. The surface photovoltage (SPV) spectrum were obtained from a measurement system containing the source of monochromatic light, a lock-in amplifier (SR830-DSP) with a light chopper (SR540). Electrochemical impedance spectra (EIS) were measured from a CHI 660E electrochemical workstation

(Chenhua Inc., Shanghai), applying a 10-mV AC signal and scanning in a frequency range between 1 MHz and 1000 Hz at different forward applied bias.

Results and Discussion

The MAPbI₃-based perovskite films were fabricated with the traditional one-step process with chlorobenzene as the antisolvent. The bare perovskite film shows a very flat surface without any large pinholes and cracks (Fig. 1a). AFM test further confirms the densely packing of perovskite crystals mostly with a size of about 500–700 nm (Fig. 1b). Crystal boundaries can be clearly observed from both the SEM and AFM images. After deposition of CdSe/LiF, the surface seems sandy and flatter, indicating that the perovskite crystals as well as their boundaries are readily covered with tiny CdSe QDs and LiF (Fig. 1c). This is also reflected from the corresponding AFM image (Fig. 1d). Some hazy boundary outlines are still observable from the SEM and AFM images, indicating that the covered CdSe/LiF double layer has a very small performance-optimized thickness. As the wurtzite phase CdSe QD has an averaged diameter of about 5.5 nm (Additional file 1: Fig. S1) and the modified LiF layer is just 0.8–1.0 nm, exact distinction of the two materials is difficult. The root mean roughness (RMS) of the film surface decreases from 10.6 nm for the bare perovskite to 4.7 nm for the CdSe/LiF deposited. Thus, fully contacted perovskite/ETL interface provides spatial convenience for electron transfer and collection through the above CdSe/LiF double layer.

The absorption properties of the films with and without CdSe/LiF layer are shown in Fig. 2a. The bare MAPbI₃ film shows a strong absorption at the entire visible region, with a typical absorption startup at about 770 nm. After depositing the CdSe/LiF on top, the film shows similar absorption tendency without much variation. Slightly increased absorption intensity in the visible light region is probably ascribed to more light scattering from the top QD layer. As the thickness of CdSe QD layer is much thinner than that of the perovskite film, the characteristic absorption of CdSe QDs (Additional file 1: Fig. S2) is not clearly exhibited.

To evaluate the charge transfer and collection ability of this novel perovskite/CdSe interface, we characterized the photoluminescence (PL) properties of different samples. The bare MAPbI₃ film on ITO glass shows a strong PL peak at about 790 nm (Fig. 2b) while this peak intensity is up to 80% quenched for the sample covered with CdSe/LiF layer. This result reflects that the photon-generated charges could be effectively separated at the perovskite/CdSe interface. Incorporation of the PEDOT:PSS anode buffer layer beneath the perovskite layer further quenches the PL intensity. For further evidence, time-resolved photoluminescence (TRPL) decay spectrum were characterized to probe the effect of inorganic buffer layer on carrier dynamics in the solar cells. For pure perovskite film, it was reported that a longer PL lifetime could be obtained through suppressing charge recombination with mixed antisolvent or surface passivation [21, 22]. Here in this work, we focused on chlorobenzene for easy comparison, although other

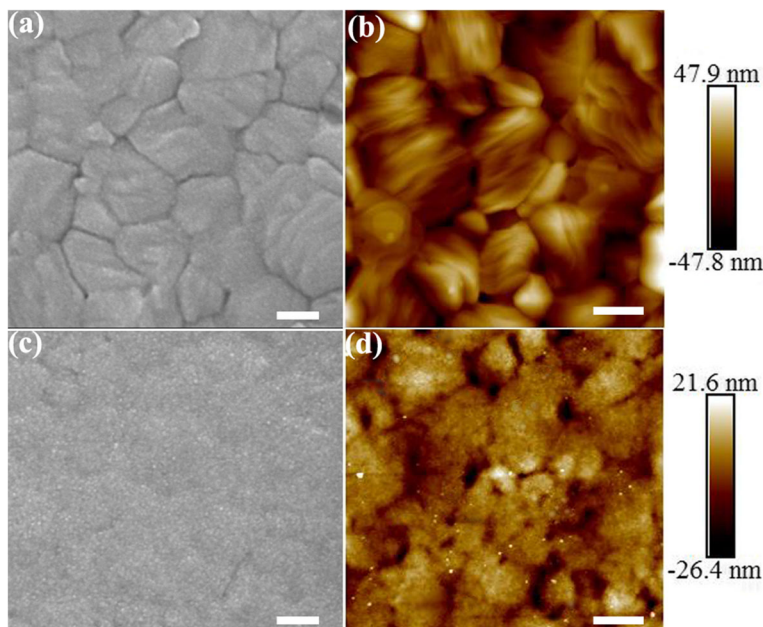


Fig. 1 SEM and AFM topology of bare perovskite film (a, b) and CdSe/LiF-covered perovskite film (c, d)

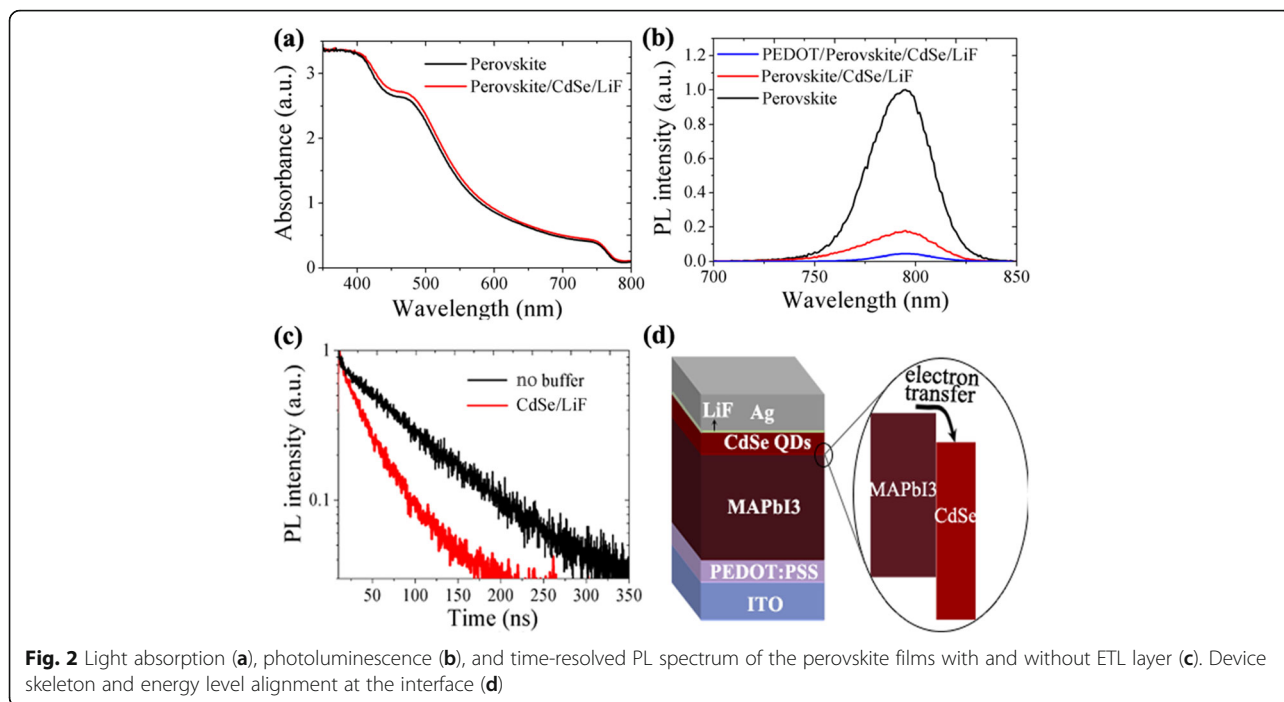


Fig. 2 Light absorption (a), photoluminescence (b), and time-resolved PL spectrum of the perovskite films with and without ETL layer (c). Device skeleton and energy level alignment at the interface (d)

antisolvent may also play a positive role in fabrication of uniform perovskite films [23]. The results in Fig. 2c show that the TRPL signal of perovskite film covered with CdSe/LiF has a faster decay as compared to the film without cathode buffer, indicating a rapid charge injection from MAPbI3 to CdSe. As shown in Fig. 2d, the perovskite/CdSe contact could form a typical type-II heterojunction that facilitates exciton dissociation and charge transfer. Thus, the results demonstrate that the adopted CdSe QDs/LiF layer is electronically beneficial to charge extraction as a cathode buffer layer. Therefore, it is highly expectable to gain a reasonable photovoltaic performance by applying the PEDOT:PSS/MAPbI3/CdSe/LiF heterostructure. The planar solar cell was thus fabricated with CdSe QDs and PEDOT:PSS as the cathode and anode buffer layer respectively, as is shown in Fig. 2d.

The photovoltaic performance of solar cell without ETL was also fabricated and measured as reference. The performance stability and repeatability of this device were found to be very poor. The best device obtained in our work generated a voltage-oriented control (V_{oc}) of 0.88 V, current density (J_{sc}) of 10 mA/cm², fill factor (FF) of 48%, and a conversion efficiency of 4.2% (Fig. 3a). Introduction of CdSe/LiF buffer layer could remarkably enhance the performance. A 10-nm CdSe QDs layer could generate greatly enhanced performance while a double layer containing 25 nm CdSe and 1 nm LiF atop produces the best target solar cells. An averaged conversion efficiency of 14.2% is achieved with a V_{oc} of 0.99 V, a J_{sc} of 20.5 mA/cm², and an FF of 69.9%. Further

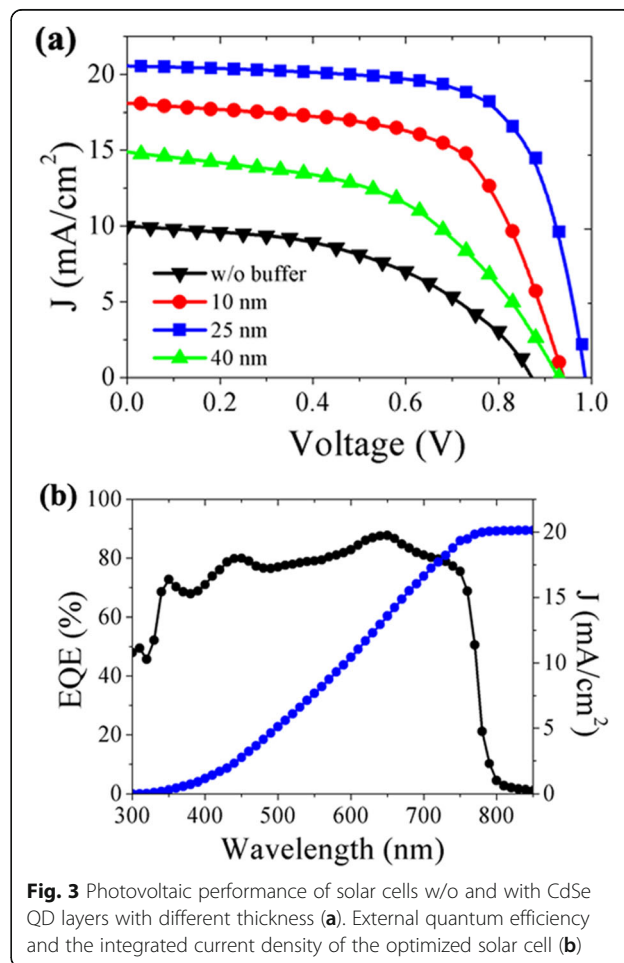


Fig. 3 Photovoltaic performance of solar cells w/o and with CdSe QD layers with different thickness (a). External quantum efficiency and the integrated current density of the optimized solar cell (b)

Table 1 Photovoltaic performance of inverted MAPbI₃ solar cells with different thickness (*T.*) of CdSe QD layer

<i>T.</i> (nm)	V _{oc} (V)	J _{sc} (mA cm ⁻²)	FF (%)	Eff (%)	R _{ss} (Ω)
0	0.88	10.0	47.7	4.2	29
10	0.94	18.1	63.5	10.8	16
25	0.99	20.5	69.9	14.2	9
40	0.93	14.9	50.0	6.9	31

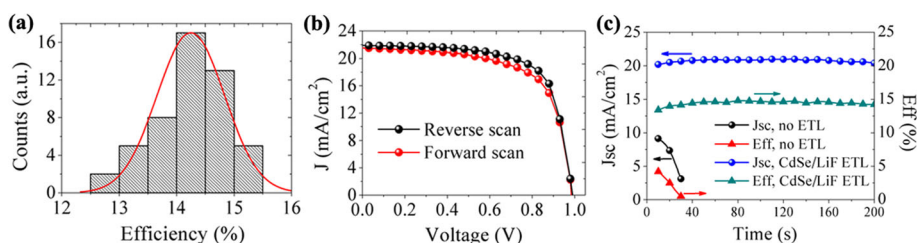
increase of the CdSe QDs layer thickness will deteriorate the performance due to largely increased series resistance (Table 1). It is noticed that this performance could only be obtained with CdSe QDs capped with pyridine. The original OA ligand always plays a detrimental role on charge transfer and collection, exhibiting an S-shaped *I-V* curve (Additional file 1: Fig. S3). The excellent photovoltaic performance from adopting CdSe/LiF buffer layer is also confirmed by the EQE results (Fig. 3b). Integration of the EQE values generates a J_{sc} value of 20.2 mA/cm² that is very close to the above measured one. It is noticed that performance obtained with our modified buffer layer is among the top values of reported perovskite solar cells with some other buffer layers [14, 15], showing the promising effectiveness of this novel ETL.

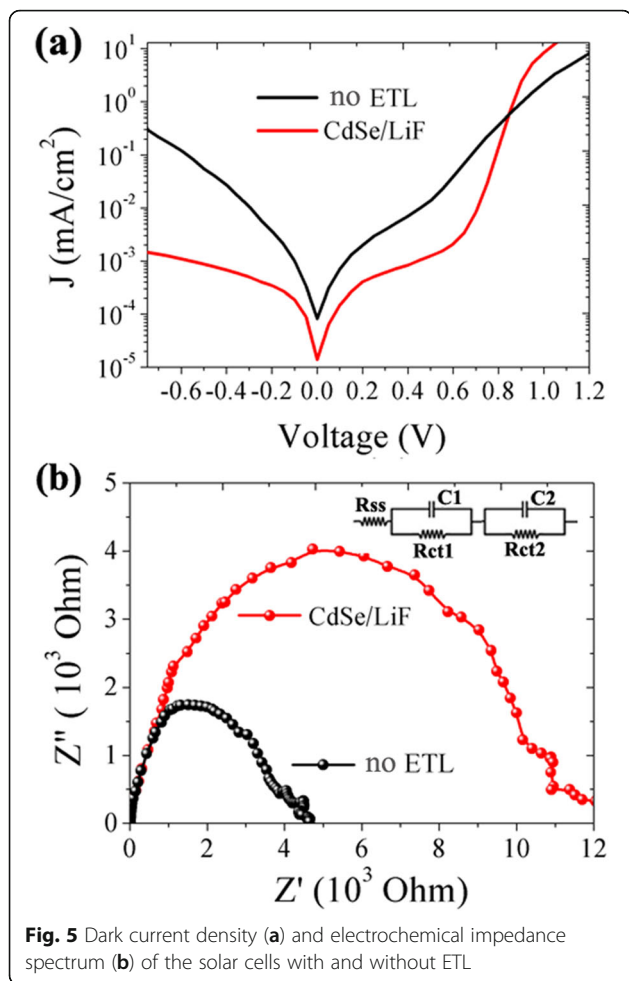
To further confirm the adaptability of the CdSe QDs/LiF layer, the performance data from over 50 devices in different batches were collected. Figure 4a shows the efficiency statistics of the obtained solar cells. The efficiency distribution is a little large with an average value of 14.2%; the best and the worst devices generate an efficiency of 15.1 and 12.7%, respectively. Normally, we synthesized fresh CdSe QDs for every batch of solar cells' fabrication. The QD quality may cause performance fluctuation among different batches because of the occasional aggregation of QDs during ligand exchange. However, near the averaged value, the solar cells exhibit a good repeatability. The best device shows no appreciable hysteresis during the reverse and forward scans (Fig. 4b). Besides, we notice this efficiency maximum of the CdSe/LiF ETL device is close to that of a traditional PCBM ETL with a maximum efficiency of 16.14%

(Additional file 1: Fig. S4). For device stability, we tracked its performance under continuous light illumination. The solar cells with CdSe/LiF show a little increase in performance at the beginning of illumination due to light-soaking effect that was commonly observed in perovskite solar cells [24, 25]. It should be noted that the *I-V* measurement was started after the initial explosion to light for about 5 s. So the performance stability was recorded after 5 s from light illumination (Fig. 4c). It can be seen that the current density as well as the conversion efficiency is stable during the light-soaking time shown, meaning that the perovskite solar cells with CdSe/LiF ETL are stable. However, without ETL covering, the solar cells show a drastical decrease during the first several seconds of illumination. This result demonstrates that our buffer layer could readily play a positive role in inhibiting moisture and oxygen that could cause fast deterioration of solar cells' performance.

As the electron extraction layer, the CdSe/LiF should efficiently collect electrons and inhibit holes from the perovskite film. Figure 5a shows the dark current density at different bias voltage. The reference device shows large current leakage due to the absence of cathode buffer layer. On the other hand, a much better rectify factor was obtained by introducing CdSe/LiF ETL and therefore, the current leakage is reduced. Further characterization on this property is carried out through electrochemistry impedance spectrum (EIS). Figure 5b shows the EIS results of the two devices under dark in an open-circuit condition. Compared to the reference, the target device shows a larger diameter of the semi-circle, that is, a larger charge recombination resistance in the perovskite film and at the perovskite/ETL interface [26, 27]. The addition of perovskite/CdSe interface could increase charge transfer recombination resistance (R_{ct}) value as shown in inset of Fig. 5b, which indicates a decreased charge recombination near the cathode. Thus, our results demonstrate an enhanced charge transfer and extraction through the CdSe/LiF ETL.

To further evaluate the charge collection ability of this buffer layer, we characterized the short-circuit current density under different light intensity and the results are

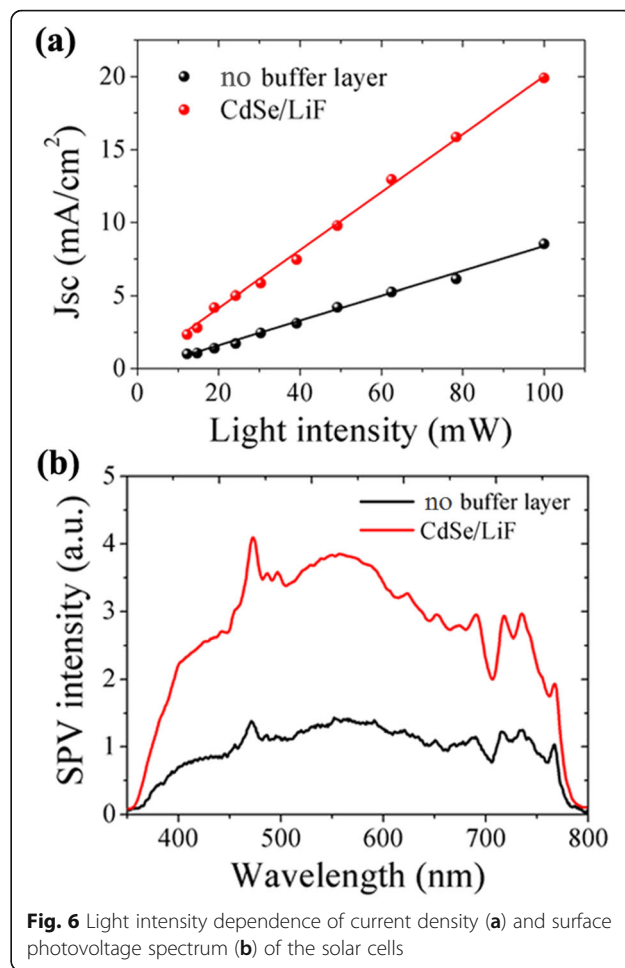
**Fig. 4** Performance statistics of the solar cells (a), *I-V* curves of the forward and reverse-can mode of the best solar cell (b) and comparison of performance stability of the solar cells with and without ETL (c)



shown in Fig. 6a. Both of the two devices show a near-linear increase in J_{sc} following the increase in light intensity. The CdSe/LiF device exhibits a much faster increase than the reference, demonstrating enhanced charge collection ability under higher light intensity. This property is also indicated from the surface photovoltage spectrum (SPV) in Fig. 6b. Without a buffer layer, the device generates relatively weak SPV signals in the visible light region, while the adoption of CdSe/LiF layer greatly enhances the SPV values in the same region. As the SPV signal is correlated with charge generation and thereafter transportation to the film surface [17, 28], the larger SPV value in the target device could be reasonably explained by the enhanced charge collection and transportation through a type-II heterojunction at the perovskite/ETL interface, as is shown in Fig. 2d.

Conclusions

In conclusion, we have fabricated planar perovskite solar cells with CdSe quantum dots/LiF electron transporting layer that is compatible to the solution process of the device. The uniform and full coverage of perovskite film



through a 25-nm CdSe QDs and 1 nm LiF would provide spacial and electronic convenience for electrons' transfer and extraction, as indicated from the TRPL, EIS, and SPV characterization and so on. The adoption of this ETL brings a significant increase in photovoltaic efficiency, from 4.8% for that without buffer layer to 14.2% in the optimized target and a maximum of 15.1%. The performance stability is also improved. Our work provides a promising candidate on ETLs for the development of highly efficient and low-cost inverted perovskite solar cells.

Additional file

Additional file 1: Figure S1. (a) TEM image of synthesized CdSe quantum dots (QDs), (b) QDs size statistics and (c) XRD pattern of synthesized CdSe QDs. The result shows a wurtzite phase of synthesized material. **Figure S2.** Light absorption of the synthesized CdSe QDs chlorobenzene solution. **Figure S3.** $I-V$ performance of solar cell with OA capped CdSe QDs. **Figure S4.** The best photovoltaic performance of perovskite solar cells with traditional PCBM as ETL.

Acknowledgements

We thank Dr. Ling Wei and Dr. Huiping Gao for their kind help on the AFM and PL measurements and discussion.

Funding

This work is supported by the National Natural Science Foundation of China (Grant no. 61306019), the Henan Provincial Science Found (Grant no. 162300410026), the Key Member of Young Teachers (Grant no. 2016GGJS-019), and the Henan University Fund.

Authors' Contributions

FRT and WZX carried out the experiments and drafted the manuscript. XDH participated in the sequence alignment. PY and LW conceived the study and participated in its design. WFZ participated in the design of the study and performed the analysis. All authors read and approved the final manuscript.

Competing Interests

The authors declare that they have no competing interests.

Publisher's Note

Springer Nature remains neutral with regard to jurisdictional claims in published maps and institutional affiliations.

Received: 26 October 2017 Accepted: 22 November 2017

Published online: 06 December 2017

References

- Yang W, Park B, Jung E, Jeon N, Kim Y, Lee D et al (2017) Iodide management in formamidinium-lead-halide-based perovskite layers for efficient solar cells. *Science* 356:1376–1379
- Tan H, Jain A, Voznyy O, Lan X, García Arquer F, Fan J et al (2017) Efficient and stable solution-processed planar perovskite solar cells via contact passivation. *Science* 355:722–726
- Zhang P, Wu J, Wang Y, Sarvari H, Liu D, Chen Z et al (2017) Enhanced efficiency and environmental stability of planar perovskite solar cells by suppressing photocatalytic decomposition. *J Mater Chem A* 5:17368–17378
- Jeng J, Chen K, Chiang T, Lin P, Tsai T, Chang Y et al (2014) Nickel oxide electrode interlayer in CH₃NH₃PbI₃ perovskite/PCBM planar-heterojunction hybrid solar cells. *Adv Mater* 26:4107–4113
- Brinkmann K, Zhao J, Pourdavoud N, Becker T, Hu T, Olthof S et al (2017) Suppressed decomposition of organometal halide perovskites by impermeable electron-extraction layers in inverted solar cells. *Nat Commun* 8:13938
- Ye S, Sun W, Li Y, Yan W, Peng H, Bian Z et al (2015) CuSCN-based inverted planar perovskite solar cell with an average PCE of 15.6%. *Nano Lett* 15:3723–3728
- Wolff C, Zu F, Paulke A, Toro L, Koch N, Neher D (2017) Reduced interface-mediated recombination for high open-circuit voltages in CH₃NH₃PbI₃ solar cells. *Adv Mater* 29:1700159
- Wang B, Zhang Z, Ye S, Gao L, Yan T, Bian Z et al (2016) Solution-processable cathode buffer layer for high-performance ITO/CuSCN-based planar heterojunction perovskite solar cell. *Electrochim Acta* 218:263–270
- Chiang C, Wu C (2016) Bulk heterojunction perovskite-PCBM solar cells with high fill factor. *Nat Photonics* 10:196–200
- Ye S, Rao H, Zhao Z, Zhang L, Bao H, Sun W et al (2017) A breakthrough efficiency of 19.9% obtained in inverted perovskite solar cells by using an efficient trap state passivator Cu(thiourea). *J Am Chem Soc* 139:7504–7512
- Zhang L, Zhang X, Yin Z, Jiang Q, Liu X, Meng J et al (2015) Highly efficient and stable planar heterojunction perovskite solar cells via a low temperature solution process. *J Mater Chem A* 3:12133–12138
- Chen W, Wu Y, Yue Y, Liu J, Zhang W, Yang X et al (2015) Efficient and stable large-area perovskite solar cells with inorganic charge extraction layers. *Science* 350:944–948
- Docampo P, Ball J, Darwiche M, Eperon G, Snaith H (2013) Efficient organometal trihalide perovskite planar-heterojunction solar cells on flexible polymer substrates. *Nat Commun* 4:2761
- Liu X, Chueh C, Zhu Z, Jo S, Sun Y, Jen A (2016) Highly crystalline Zn₂SnO₄ nanoparticles as efficient electron-transporting layers toward stable inverted and flexible conventional perovskite solar cells. *J Mater Chem A* 4:15294–15301
- You J, Meng L, Song T, Guo T, Yang Y, Chang W et al (2016) Improved air stability of perovskite solar cells via solution-processed metal oxide transport layers. *Nat Nanotechnol* 11:75–81
- Peng X, Manna L, Yang W, Wickham J, Scher E, Kadavanich A et al (2000) Shape control of CdSe nanocrystals. *Nature* 404:59–61
- Tan F, Wang Z, Qu S, Cao D, Liu K, Jiang Q et al (2016) A CdSe thin film: a versatile buffer layer for improving the performance of TiO₂ nanorod array: PbS quantum dot solar cells. *Nano* 8:10198–10204
- Zhao T, Goodwin E, Guo J, Wang H, Diroll B, Murray C et al (2016) Advanced architecture for colloidal PbS quantum dot solar cells exploiting a CdSe quantum dot buffer layer. *ACS Nano* 10:9267–9273
- Gao D, Helander M, Wang Z, Pozzo D, Greiner M, Lu Z (2010) C₆₀LiF blocking layer for environmentally stable bulk heterojunction solar cells. *Adv Mater* 22:5404–5408
- Tang Z, George Z, Ma Z, Bergqvist J, Tvingstedt K, Vandewal K et al (2012) Semi-transparent tandem organic solar cells with 90% internal quantum efficiency. *Adv Energy Mater* 2:1467–1476
- Wang Y, Wu J, Zhang P, Liu D, Zhang T, Ji L et al (2017) Stitching triple cation perovskite by a mixed anti-solvent process for high performance perovskite solar cells. *Nano Energy* 39:616–625
- Li S, Zhang P, Wang Y, Sarvari H, Liu D, Wu J et al (2017) Interface engineering of high efficiency perovskite solar cells based on ZnO nanorods using atomic layer deposition. *Nano Res* 10:1092–1103
- Ji L, Zhang T, Wang Y, Zhang P, Liu D, Chen Z et al (2017) Realizing full coverage of stable perovskite film by modified anti-solvent process. *Nanoscale Res Lett* 12:367
- Zhao C, Chen B, Qiao X, Luan L, Lu K, Hu B (2015) Revealing underlying processes involved in light soaking effects and hysteresis phenomena in perovskite solar cells. *Adv Energy Mater* 5:1500279
- Nie W, Blancon J, Neukirch A, Appavoo K, Tsai H, Chhowalla M et al (2016) Light-activated photocurrent degradation and self-healing in perovskite solar cells. *Nat Commun* 7:11574
- Christians J, Fung R, Kamat R (2014) An inorganic hole conductor for organo-lead halide perovskite solar cells. Improved hole conductivity with copper iodide. *J Am Chem Soc* 136:758–764
- Jung J, Chueh C, Jen A (2015) A low-temperature, solution-processable, Cu-doped nickel oxide hole-transporting layer via the combustion method for high-performance thin-film perovskite solar cells. *Adv Mater* 27:7874–7880
- Barnea-Nehoshtan L, Kirmayer S, Edri E, Hodes G, Cahen D (2014) Surface photovoltage spectroscopy study of organo-lead perovskite solar cells. *J Phys Chem Lett* 5:2408–2413

Submit your manuscript to a SpringerOpen® journal and benefit from:

- Convenient online submission
- Rigorous peer review
- Open access: articles freely available online
- High visibility within the field
- Retaining the copyright to your article

Submit your next manuscript at ► springeropen.com